Springer

KSME

Journal of Mechanical Science and Technology 26 (10) (2012) 3231~3242
www.springerlink.com/content/1738-494x
DOI 10.1007/s12206-012-0823-7

A DXDR large deflection analysis of uniformly loaded square, circular and elliptical orthotropic plates using non-uniform rectangular finite-differences †

M. Kadkhodayan[1,*], A. Erfani Moghadam[1], G.J. Turvey[2] and J. Alamatian[3]

[1]*Department of Mechanical Engineering, The University of Ferdowsi, 91775-1111, Mashhad, Iran*
[2]*Engineering Department, Lancaster University, Bailrigg, Lancaster LA1 4YR, U.K.*
[3]*Department of Civil Engineering, Azad University, Mashhad, Iran*

(Manuscript Received October 17, 2011; Revised January 27, 2012; Accepted April 30, 2012)

Abstract

A finite-difference analysis of the large deflection response of uniformly loaded square, circular and elliptical clamped and simply-supported orthotropic plates is presented. Several types of non-uniform (graded) mesh are investigated and a mesh suited to the curved boundary of the orthotropic circular and elliptical plate is identified. The DXDR method–a variant of the DR (dynamic relaxation) method–is used to solve the finite-difference forms of the governing orthotropic plate equations. The DXDR method and irregular rectilinear mesh are combined along with the Cartesian coordinates to treat all types of boundaries and to analyze the large deformation of non-isotropic circular/elliptical plates. The results obtained from plate analyses demonstrate the potential of the non-uniform meshes employed and it is shown that they are in good agreement with other results for square, circular and elliptical isotropic and orthotropic clamped and simply-supported plates in both fixed and movable cases subjected to transverse pressure loading.

Keywords: Orthotropic circular and elliptical plates; Non-uniform rectangular mesh; Large deflection; Dynamic relaxation

1. Introduction

The increasing use of composite materials in thin-walled structures, which may be regarded as assemblies of plate and shell elements, provides both the catalyst and justification for the continual development and refinement of numerical procedures for the solution of orthotropic and other plate flexure problems. The solutions of particular interest here are for the large deflection response of clamped and simply-supported circular and elliptical plates with rectangular Cartesian orthotropy. Such plates commonly arise in practice as inspection covers and other types of end closures.

Both the small and large deflection responses of orthotropic plates have been investigated by a number of researchers during the course of the past half-century. For example, in the 1970's Chia [1, 2] studied the nonlinear flexural behavior of rectangular orthotropic plates using an approximate analytical solution. Dalaei and Kerr [3] investigated the small deflection response of clamped rectangular orthotropic plates subjected to uniform transverse pressure using the extended Kantorovich method. In later studies, Mbakogu and Pavlovica [4] and Tabalov et al. [5] also investigated the small deflection response of clamped rectangular orthotropic plates. Mistou et al. [6] investigated the behavior of clamped laminated rectangular orthotropic plates subjected to uniform transverse pressure both experimentally and numerically using a Ritz approximate analysis. Bhaskar and Kaushik [7] used a double Fourier series approach to analyze unsymmetric cross-ply laminated clamped rectangular plates. Recently, Salehi and Sobhani [8] used Mindlin plate theory in conjunction with the DR method to investigate both the small and large deflection response symmetrically laminated fiber-reinforced sector plates.

In the majority of the aforementioned papers the plate was either of rectangular or circular geometry. Therefore, for numerical mesh-based solutions, a uniform square or rectangular mesh would be adequate for rectangular plates with rectangular Cartesian orthotropy. Similarly, for circular plates with polar orthotropy, an orthogonal polar mesh would suffice but would not readily accommodate rectangular Cartesian orthotropy. Here, however, the focus of interest is on the use of a single non-uniform rectangular mesh that may be used to analyze square, circular and elliptical plates with rectangular Cartesian orthotropy.

It is the main objective of the current study to show if the DXDR method and irregular rectilinear mesh are combined along with the Cartesian coordinates one can treat all types of

*Corresponding author. Tel.: +98 9153111869, Fax.: +98 511 8763304
E-mail address: kadkhoda@um.ac.ir
† Recommended by Associate Editor Heung Soo Kim

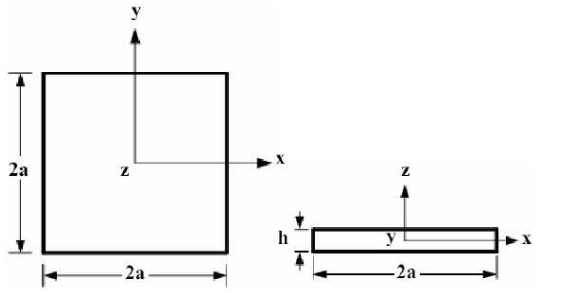

(a) (b)

Fig. 1. Square plate with its principal axes of orthotropy parallel to the x and y axes: (a) plan view; (b) cross-section.

boundaries which is also extendable to the large deformation of non-isotropic plates. The main application of the current method can be the analysis of orthotropic materials which are made initially in rectangular dies and the fibers are inserted in rectilinear dictions and then are cut into circular and elliptical forms.

The large deflection response of clamped and simply-supported square, circular and elliptical orthotropic plates subjected to uniform transverse pressure is investigated using several types of non-uniform rectangular finite-difference mesh. Consequently, the same governing equations may be used for square, circular and elliptical plates. Moreover, the mesh could be used to analyze orthotropic plates with more general boundary shapes.

A variant of the DR method, namely the DXDR method [9] is employed to solve the finite-difference forms of the large deflection orthotropic plate equations. The results are presented for both deflections and stress couples in order to demonstrate the accuracy of the present non-uniform mesh large deflection solutions by comparison with counterpart solutions obtained with uniform meshes and by other approximate analysis techniques.

2. Mesh generation

Consider a square orthotropic plate with sides of length $2a$ and thickness h, as shown in Fig. 1. For convenience, the origin of the co-ordinate system x, y, z is located at the center of the mid-plane of the plate. In order to carry out a finite-difference analysis of a square or rectangular plate it is generally sufficient to use a uniform square or rectangular mesh extending over the plate domain. However, for plates with curved boundaries it is not usually possible to use a uniform square or regular rectangular mesh because the nodes of the mesh do not coincide with curved boundary of the plate.

Different types of non-uniform rectangular meshes may be generated in either or both of the co-ordinate directions x and y. The mesh may be uniform in one direction and non-uniform in the other direction. In this case the mesh is denoted as a Type 1 mesh. Fig. 2(a) shows an example of a Type 1 mesh, in which the mesh is uniform in the y direction and non-uniform in the x direction. Here, the mesh size in the

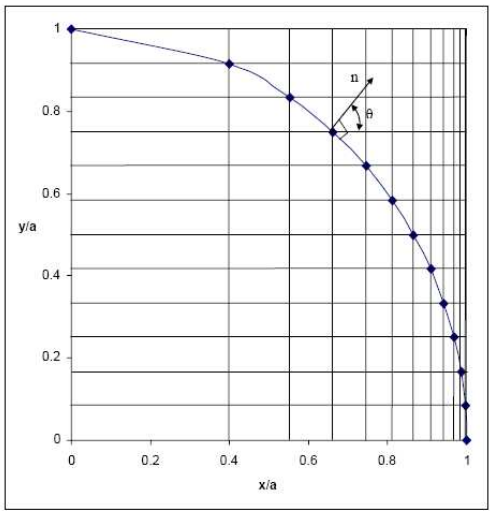

(a)

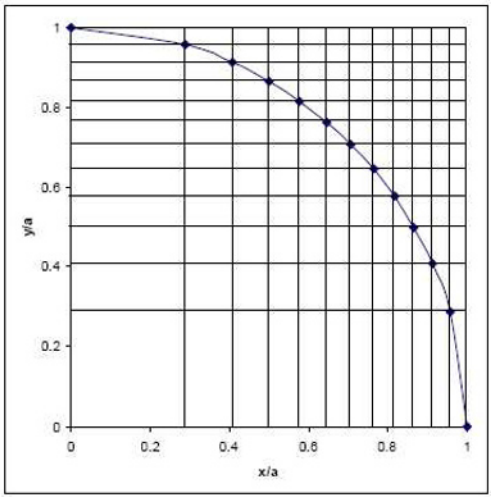

(b)

Fig. 2. Examples of non-uniform meshes: (a) uniform in the y direction $n_y = 1$ and non-uniform in the x direction $n_x \neq 1$ [Type 1]; (b) non-uniform in both x and y directions $\left(n_x = n_y = 0.5\right)$ [Type 2].

x direction reduces as the nodal distance from the center of the plate increases (it is assumed that symmetry is exploited and only the positive quadrant of the plate is modeled). Clearly, the mesh may be arranged to be non-uniform with respect to both co-ordinate directions. One example of these non-uniform meshes, designated Type 2, is illustrated in Fig. 2(b). Such non-uniform bi-directional meshes may be generated in a variety of ways. Here, simple power laws are employed. The co-ordinates of the nodes of the mesh in the x and y directions are defined as follows:

$$x = a\left(\frac{i}{k}\right)^{n_x} \tag{1a}$$

$$y = a\left(\frac{j}{k}\right)^{n_y} . \tag{1b}$$

In Eq. (1) a is the half side length of the square plate or the radius of the circular plate, i and j are the node numbers in the x and y directions, respectively, where $0 \le i, j \le k$, $k+1$ is the total number of nodes in the x and y directions, respectively, and n_x and n_y are both positive constants. If one of the constants n_x or n_y is equal to one and the other is not equal to one, then a Type 1 mesh is defined, i.e. $n_x = 1$ and $n_y \neq 1$ or $n_x \neq 1$ and $n_y = 1$. On the other hand, the mesh will be non-uniform in both x and y directions when $n_x = 1$ and $n_y \neq 1$. Moreover, when $n_x = n_y = 1$, a uniform mesh with respect to both the x and y axes is defined.

For plates with a curved boundary, n_x and n_y cannot be selected independently. In other words, these quantities must be determined so that the mesh nodes coincide with curved boundary of the plate. For example, the boundary nodes of a circular plate must satisfy following equation:

$$x^2 + y^2 = a^2 \tag{2}$$

where a is the radius of plate. Substituting Eqs. (1a) and (1b) into Eq. (2) leads to the following result:

$$\left(\frac{i}{k}\right)^{2n_x} + \left(\frac{j}{k}\right)^{2n_y} = 1 . \tag{3}$$

For a Type 1 mesh (uniform in one direction and non-uniform in the other direction), the unknown power n_x or n_y in the non-uniform direction may be determined by solving Eq. (3). In other words, n_x (or n_y) is determined so that the mesh lines intersect the circle boundary. It is clear that n_x (or n_y) will have a specific value for each mesh line. However, a Type 2 mesh is defined by $n_x = n_y = 0.5$, where the mesh has the same degree of non-uniformity in both the x and y directions. Other values of n_x and n_y, between 0 and 1 or greater than 1, are unlikely to be of interest because they only increase the rate of directional non-uniformity of the mesh. In such cases, n_x and n_y would have different values for each line of the mesh for the other values, i.e. when $n_x \neq n_y \neq 0.5$. Nevertheless, for the sake of completeness, they are investigated to a limited extent and discussed later in the paper.

Similar remarks apply to other plates with curvilinear boundaries, e.g. elliptical plates. In order to investigate the accuracy of these meshes, the circular and elliptical forms of Eq. (3) are used first to generate meshes for square and rectangular plates, respectively. This mesh generation method may be explained by a simple example. Consider a square plate of side length $2a$. To define a Type 1 mesh over a square plate, a circle of radius a with its center at the center of the square plate is defined, as shown in Fig. 2(a). Then, a Type 1 mesh is generated in one direction (x or y) over the circle by, for example, setting $n_x = 1$ and determining n_y from Eq. (3). Here, the total number of mesh nodes in the x and y directions is assumed to be 13 (k = 12). The mesh lines over circle are then extended to the sides of the square to produce a Type 1 mesh over the square plate. Other mesh types (for example, Type 2 mesh which is shown in Fig. 2(b)), may be generated in a similar manner. For rectangular plates, an inscribed ellipse should be used. To demonstrate the mesh distribution in the current study, the used mesh for the circular and elliptical plates are shown in Figs. 3(a) and 3(b), respectively.

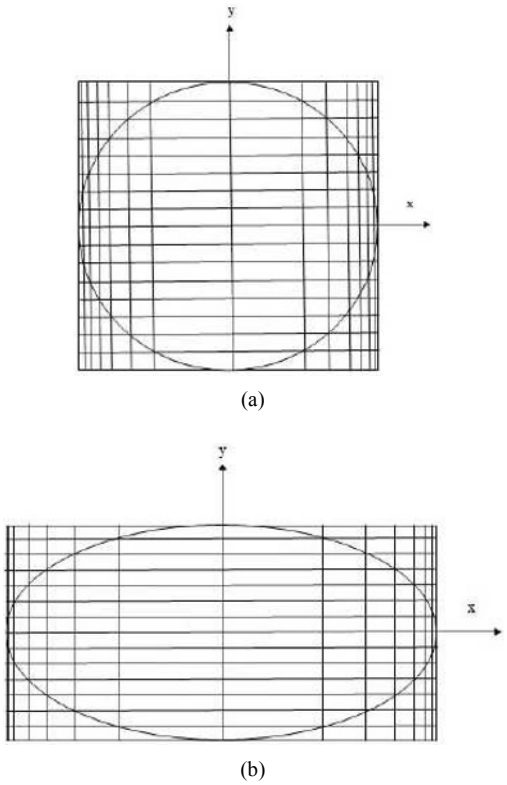

Fig. 3. The general form of mesh distribution of: (a) circular plate; (b) elliptical plate.

3. Governing orthotropic plate equations

The Cartesian forms of the equilibrium equations for an orthotropic plate may be written in the following form [10]:

$$\frac{\partial N_x}{\partial x} + \frac{\partial N_{xy}}{\partial y} = 0 \tag{4}$$

$$\frac{\partial N_y}{\partial y} + \frac{\partial N_{xy}}{\partial x} = 0 \tag{5}$$

$$\frac{\partial^2 M_x}{\partial x^2} + 2\frac{\partial^2 M_{xy}}{\partial x \partial y} + \frac{\partial^2 M_y}{\partial y^2} + N_x \frac{\partial^2 w}{\partial x^2} + 2N_{xy}\frac{\partial^2 w}{\partial x \partial y} + N_y \frac{\partial^2 w}{\partial y^2} + q = 0 . \tag{6}$$

It should be appreciated that Eqs. (4) and (5) are the in-plane equilibrium equations and Eq. (6) is the out-of-plane equilibrium equation. In these equations, N_x, N_y and N_{xy} are the stress resultants, M_x, M_y and M_{xy} are the stress couples, w is the deflection and q is the transverse pressure.

The stress resultants and stress couples may be expressed as:

$$\left(N_x, N_y, N_{xy}\right) = \int_{-\frac{h}{2}}^{\frac{h}{2}} \left(\sigma_x, \sigma_y, \tau_{xy}\right) dz \tag{7a}$$

$$\left(M_x, M_y, M_{xy}\right) = \int_{-\frac{h}{2}}^{\frac{h}{2}} z\left(\sigma_x, \sigma_y, \tau_{xy}\right) dz \,. \tag{7b}$$

In Eq. (7) σ_x, σ_y and τ_{xy} are the direct and shear stress components.

The stresses under the integrals on the right-hand sides of Eq. (7) are given in Ref. [11] as:

$$\begin{bmatrix} \sigma_x \\ \sigma_y \\ \tau_{xy} \end{bmatrix} = \begin{bmatrix} Q_{11} & Q_{12} & 0 \\ Q_{12} & Q_{22} & 0 \\ 0 & 0 & Q_{66} \end{bmatrix} \begin{bmatrix} \varepsilon_x \\ \varepsilon_y \\ \gamma_{xy} \end{bmatrix} . \tag{8}$$

In Eq. (8), ε_x, ε_y and γ_{xy} are the direct and shear strains and the terms $Q_{ij}\left(i, j = 1, 2, 6\right)$ are the reduced stiffness which may be expressed as:

$$Q_{11} = \frac{E_{11}}{\left(1 - \upsilon_{12}\,\upsilon_{21}\right)} \tag{9a}$$

$$Q_{12} = \frac{\upsilon_{12}\,E_{22}}{\left(1 - \upsilon_{12}\,\upsilon_{21}\right)} = \frac{\upsilon_{21}\,E_{11}}{\left(1 - \upsilon_{12}\,\upsilon_{21}\right)} \tag{9b}$$

$$Q_{22} = \frac{E_{22}}{\left(1 - \upsilon_{12}\,\upsilon_{21}\right)} \tag{9c}$$

$$Q_{66} = G_{12} \,. \tag{9d}$$

In Eq. (9), E_{11} and E_{22} are the elastic moduli with respect to the major and minor axes of orthotropy, respectively, and G_{12} is the shear modulus with respect to the same axes. For orthotropic plates, which are considered here, the principal axes of orthotropy coincide with the x and y axes. The terms υ_{12} and υ_{21} denote the major and minor Poisson's ratios.

The strains of points at a distance z above the mid-plane of the plate are given as:

$$\begin{bmatrix} \varepsilon_x \\ \varepsilon_y \\ \gamma_{xy} \end{bmatrix} = \begin{bmatrix} \varepsilon_x^0 \\ \varepsilon_y^0 \\ \gamma_{xy}^0 \end{bmatrix} + z \begin{bmatrix} k_x^0 \\ k_y^0 \\ k_{xy}^0 \end{bmatrix} . \tag{10}$$

In Eq. (10) ε_x^0, ε_y^0 and γ_{xy}^0 are the direct and shear strain of the plate mid-plane and k_x^0, k_y^0 and k_{xy}^0 are the curvatures and twist of the plate mid-plane.

The relationships between the mid-plane strains and displacements are given as:

$$\varepsilon_x^0 = \frac{\partial u}{\partial x} + \frac{1}{2}\left(\frac{\partial w}{\partial x}\right)^2 \tag{11a}$$

$$\varepsilon_y^0 = \frac{\partial v}{\partial y} + \frac{1}{2}\left(\frac{\partial w}{\partial y}\right)^2 \tag{11b}$$

$$\gamma_{xy}^0 = \frac{\partial u}{\partial y} + \frac{\partial v}{\partial x} + \frac{\partial w}{\partial x}\frac{\partial w}{\partial y} \,. \tag{11c}$$

In Eq. (11) u and v are the in-plane displacements in the x and y directions, respectively. Moreover, it should also be appreciated that geometric nonlinearity, due to stretching of the plate mid-plane, is reflected by the presence of the quadratic terms in Eq. (11).

Similar relationships exist between the mid-plane curvatures and deflection of the plate as follows:

$$k_x^0 = -\frac{\partial^2 w}{\partial x^2} \tag{12a}$$

$$k_y^0 = -\frac{\partial^2 w}{\partial y^2} \tag{12b}$$

$$k_{xy}^0 = -2\frac{\partial^2 w}{\partial x\,\partial y} \,. \tag{12c}$$

The boundary conditions in the plate analyses for the square plate are:

(a) Fixed clamped edge

Along $x = \pm a$:

$$u = 0, \quad v = 0, \quad w = 0, \quad \frac{\partial w}{\partial x} = 0 \,. \tag{13a}$$

Along $y = \pm a$:

$$u = 0, \quad v = 0, \quad w = 0, \quad \frac{\partial w}{\partial y} = 0 \,. \tag{13b}$$

(b) Movable clamped edge

Along $x = \pm a$:

$$v = 0, \quad w = 0, \quad N_x = 0, \quad \frac{\partial w}{\partial x} = 0 \,. \tag{13c}$$

Along $y = \pm a$:

$$u = 0, \quad w = 0, \quad N_y = 0, \quad \frac{\partial w}{\partial y} = 0 \,. \tag{13d}$$

(c) Fixed simply-supported edge
Along $x = \pm a$:

$$u = 0, \quad v = 0, \quad w = 0, \quad M_x = 0 . \tag{13e}$$

Along $y = \pm a$:

$$u = 0, \quad v = 0, \quad w = 0, \quad M_y = 0 . \tag{13f}$$

(d) Movable simply-supported edge
Along $x = \pm a$:

$$v = 0, \quad w = 0, \quad M_x = 0, \quad N_x = 0 . \tag{13g}$$

Along $y = \pm a$:

$$u = 0, \quad w = 0, \quad M_y = 0, \quad N_y = 0 . \tag{13h}$$

Because both the plate geometry and the loading are symmetric about the x and y axes only one quarter of the plate has to be analyzed. It is clear that w, N_x, N_y, M_x and M_y are symmetric about the x and y axes, M_{xy} is antisymmetric about the x and y axes, u is symmetric about the x axis and antisymmetric about the y axis and υ is antisymmetric about the x axis and symmetric about the y axis. Hence, the foregoing symmetry/antisymmetry conditions have to be enforced along the x and y axes.

In the case of the circular and elliptical plates, the same symmetry/antisymmetry conditions have to be enforced along the x and y axes. However, along the circumferential boundary the conditions are somewhat more complicated. For example in the fixed clamped boundary condition, at all nodal points around the circumference of the plate u, v and w are set to zero. In addition, the slope normal to the circumference, i.e. in the n direction (see Fig. 2(a)), has also to be set to zero. This boundary condition is defined as:

$$\frac{\partial w}{\partial n} = \frac{\partial w}{\partial x}\frac{\partial x}{\partial n} + \frac{\partial w}{\partial y}\frac{\partial y}{\partial n} = \frac{\partial w}{\partial x}\cos\theta + \frac{\partial w}{\partial y}\sin\theta . \tag{13i}$$

In Eq. (13i) the angle θ is defined as shown in Fig. 2(a). It is easy to show that the condition for simply-supported cases (fixed and movable) would be:

$$M_n = 0 \;\Rightarrow\; \frac{\partial^2 w}{\partial n^2} = 0 \;\Rightarrow\; \frac{\partial^2 w}{\partial x^2}\cos^2\theta + 2\frac{\partial^2 w}{\partial x \partial y}\sin\theta\cos\theta + \frac{\partial^2 w}{\partial y^2}\sin^2\theta = 0 . \tag{13j}$$

Moreover, the condition for movable cases (simply-supported and clamped) is:

$$\left(\sigma_n = 0\right)_{membrane} \quad \& \quad \varepsilon_t = 0 \;\Rightarrow\; \frac{\partial u}{\partial n} = 0 \;\Rightarrow\; \frac{\partial u}{\partial x}\cos\theta + \frac{\partial u}{\partial y}\sin\theta = 0 . \tag{13k}$$

4. DXDR solution of the governing large deflection orthotropic plate equations

The DXDR method is a modified version of the original DR method. In this modified method the starting vector and damping factor are selected more deliberately compared to the original DR [12]. It is an iterative time-stepping solution technique for modeling the response of damped dynamic systems. However, it has mainly been used to obtain the static response by artificially damping out the oscillations of equivalent quasi-dynamic systems. The starting point of any DXDR analysis to determine the static structural response is the formulation of the quasi-dynamic system of governing equations. Thus, the second-order quasi-dynamic plate equations describing the large deflection response of the square, circular and elliptical orthotropic plates, i.e. Eqs. (4)-(6), may be expressed as follows for the n^{th} time increment [12]:

$$m_{ii}^n \ddot{D}_i^n + c_{ii}^n \dot{D}_i^n + f_i^n = p_i^n \tag{14}$$

where $\dot{D}_i^n$ and $\ddot{D}_i^n$ are (3×1) vectors of velocity and acceleration, f_i^n and p_i^n are vectors of the internal forces (corresponding principally to the LHS's of Eqs. (4)-(6)) and the applied pressure q at the i^{th} node and m_{ii}^n and c_{ii}^n are (3×3) diagonal mass and damping matrices for the three displacement components u, v and w at node i during the n^{th} iteration, respectively.

Now, because only the static large deflection response of the orthotropic plate is of interest, Eq. (14) may be transformed into time-stepping initial value format for the plate velocities [12]. The equation then becomes:

$$\dot{D}_i^{\,n+\frac{1}{2}} = \frac{\left(2-\tau^n \varsigma_i^n\right)}{\left(2+\tau^n \varsigma_i^n\right)} \dot{D}_i^{\,n-\frac{1}{2}} + \frac{2\tau^n}{\left(2+\tau^n \varsigma_i^n\right)} \frac{r_i^n}{m_{ii}^n} . \tag{15}$$

In Eq. (15), τ^n is the fictitious time step, ς_i^n are the nodal damping factors and $r_i^n = \left(p_i^n - f_i^n\right)$ is the force vector at node i.

The nodal displacements D_i^{n+1} are determined from the velocities calculated in Eq. (15) by means of the following simple integration rule:

$$D_i^{n+1} = D_i^n + \tau^{n+1} \dot{D}_i^{\,n+\frac{1}{2}} . \tag{16}$$

Furthermore, it is convenient to relate the damping and mass matrices as follows [12]:

$$c_{ii} = \varsigma_i^n m_{ii} . \tag{17}$$

In the DXDR method, the mass matrix, nodal damping factors and the time increment should be defined in such a way as to guarantee the stability and convergence of the iterative procedure. The most common method of achieving this objective is to determine m_{ii} by means of Gerschgörin theorem. According to this theorem, the following inequality must be satisfied in order to guarantee the stability of the iterations [13]:

$$m_{ii}^n \geq \frac{\left(\tau^n\right)^2}{4} \sum_{j=1}^{k} \left| S_{ij,T}^n \right| . \tag{18}$$

In Eq. (18) k is the number of degrees of freedom of the structure and $S_{ij,T}^n$ is the ij^{th} element of the tangent stiffness matrix during the n^{th} iteration and is given by:

$$S_{ij,T}^n = \frac{\partial f_i^n}{\partial D_j} . \tag{19}$$

Alternatively, by applying Rayleigh's Principle [14] at each node, the instantaneous critical damping factor for node i during the n^{th} iteration [12] may be expressed as:

$$\varsigma_i^n = 2 \left\{ \frac{\left(D_i^n\right)^T f_i D_i^n}{\left(D_i^n\right)^T m_{ii}^n D_i^n} \right\}^{\frac{1}{2}} . \tag{20}$$

Other approaches have also been suggested [13]. The fictitious time increment of the n^{th} iteration is usually assumed to be constant and equal to unity. However, some researchers have proposed that this parameter should also be based on the Rayleigh quotient [15]. Techniques have also been proposed to determine the initial displacement vector in order to reduce the computational time [12, 16, 17].

5. Large deflection results for square, circular and elliptical plates using non-uniform meshes

Different results are presented in this section. The total number of nodes in the x and y directions, is equal to 13 (k = 12). The first set of results has been computed for a square clamped isotropic plate subjected to uniform transverse pressure loading. The results are intended to demonstrate that converged and accurate deflections can be obtained with non-uniform finite-difference meshes. In Fig. 4 the plate center deflections with Type 1 and Type 2 non-uniform meshes are compared with deflections obtained from Chia's [18] approximate analytical solution. It is clear that the center deflections obtained for both meshes are in reasonably good agreement with the deflections predicted by Chia's approximate analytical solution.

Table 1. Elastic constants for the three types of orthotropic materials used in the large deflection plate analyses.

Elastic constants	Glass-epoxy	Graphite-epoxy	Boron-epoxy
E11/E22	3	40	10
G12/E22	0.5	0.6	0.33
υ_{12}	0.25	0.25	0.22

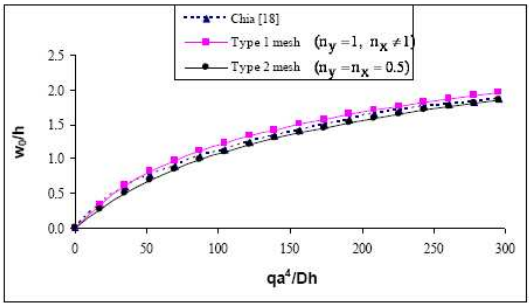

Fig. 4. Comparison of load-center deflection responses of clamped square isotropic plates.

A second set of comparison analyses has been undertaken for clamped square orthotropic plates subjected to uniform transverse pressure in order to demonstrate that the DXDR analysis produces converged and accurate results for orthotropic materials. For these comparisons it has been necessary to define the elastic moduli of the orthotropic plate materials to be used in the analyses. Three materials were selected with properties representative of unidirectional glass, carbon and boron fiber reinforced polymers. The elastic constants, non-dimensionalized with respect to the minor elastic modulus, are presented in Table 1.

The pressure-center deflection responses of glass-epoxy, carbon-epoxy and boron-epoxy plates are presented in Figs. 5(a), 5(b) and 5(c), respectively. Again, Chia's [18] approximate analytical solution is used as the benchmark solution for the comparison. It is evident that the center deflections predicted with the Type 1 mesh (non-uniform in the x direction) are in closer agreement with Chia's [18] values than the center deflections predicted with the Type 2 mesh (non-uniform in both directions). It is presumed that the additional non-uniformity of the mesh is responsible for the underestimation of the center deflection response by the Type 2 mesh. It has to be pointed out here that in orthotropic plates the dependency of results to the type of mesh is more severe than that for the isotropic plates. However, using the Type 1 mesh is always more reliable in all cases.

In order to examine further the differences between the results obtained with both uniform and non-uniform meshes, the stress couple distribution along the x axis is computed for a square glass-epoxy clamped plate when the major orthotropic axis is normal to the x axis. It is clear that there is very good agreement between the stress couples for both uniform and Type 1 non-uniform meshes. The Type 2 non-uniform mesh appears to predict significantly smaller (in the negative sense) values for

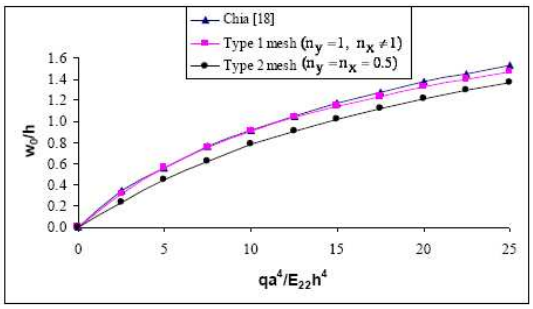

(a)

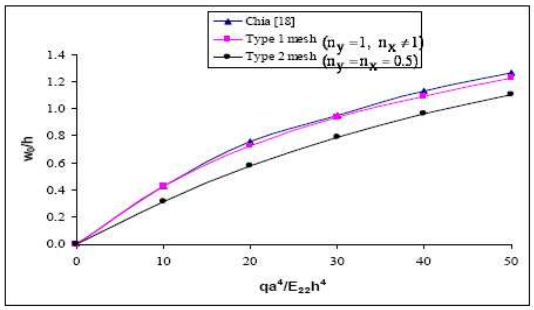

(b)

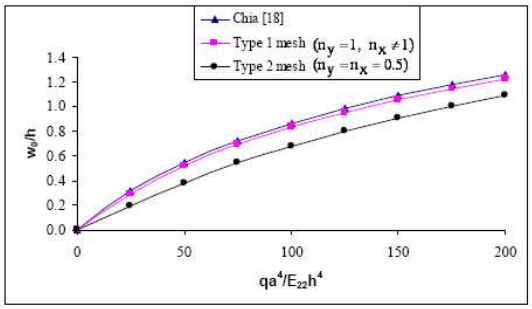

(c)

Fig. 5. Comparison of load-center deflection responses of square orthotropic clamped plates subjected to uniform transverse pressure (computed using Type 1 and 2 meshes): (a) glass-epoxy plate; (b) carbon-epoxy plate; (c) boron-epoxy plate.

the stress couple when $x/a \geq 0.7$, as shown in Fig. 6.

It is perhaps worth emphasizing that in the Type 1 mesh analysis, shown in Fig. 6, the major orthotropic axis was parallel to y axis (the uniform mesh direction). This choice of direction for the major orthotropic axis may be justified by comparing the results obtained for the deflection profiles along the x and y axes. The clamped square orthotropic plate was re-analyzed twice with both the uniform and non-uniform Type 1 meshes, i.e. once with the major axis of orthotropy parallel to the y axis and once with major axis parallel to the x axis. It is clear from the deflection profiles along the x and y axes, shown in Fig. 7, that the results obtained with the major axis of orthotropy parallel to the y axis are more accurate. It is well known that for orthotropic plates subjected to uniform transverse pressure over the central region of the plate the deflection profile is flatter transverse to the principal orthotropic axis than it is parallel to this axis [18]. Moreover, for the Type 1 mesh, with the principal axis of orthotropy in the y direction, the mesh in the x direction, i.e. transverse to the major orthotropic axis, is coarser nearer to the center and finer nearer the edge of the plate. Hence, because the mesh is coarser in the flat region of the plate, the error is smaller than if the coarse mesh is used in the direction of the major orthotropic axis (the y direction).

Other non-uniform meshes may be generated by using different values of the exponent n_y in Eq. (1b). Square glass-epoxy clamped plates subjected to uniform transverse pressure

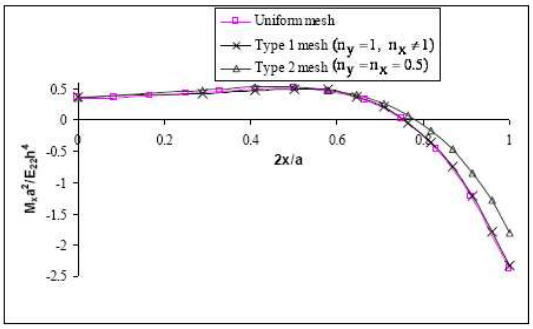

Fig. 6. Comparison of stress couple profiles along the x axis of a square glass-epoxy plate subjected to uniform transverse pressure (computed using uniform and Type 1 and 2 meshes) – principal axis of orthotropy parallel to the y axis.

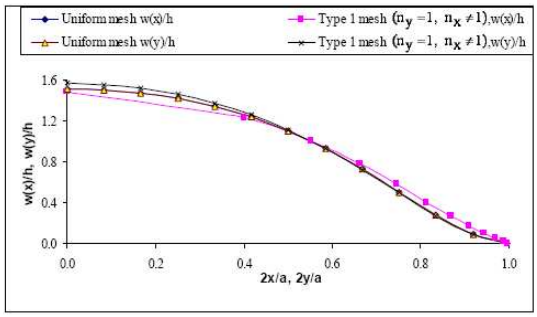

(a)

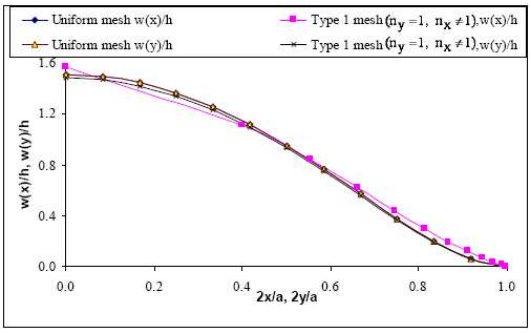

(b)

Fig. 7. Deflection profiles along the x and y axes of square orthotropic clamped plates subjected to uniform transverse pressure computed using uniform and Type 1 meshes: (a) major axis of orthotropy in the x direction; (b) major axis of orthotropy in the y direction.

Table 2. The n_x values corresponding to each mesh line for n_y = 1.2, 1.3 and 1.4 (k = 12).

i	j	n_x		
		$n_y = 1.2$	$n_y = 1.3$	$n_y = 1.4$
0	12	1	1	1
1	11	0.335796	0.321378	0.308149
2	10	0.289474	0.271840	0.255832
3	9	0.250980	0.231254	0.213571
4	8	0.216027	0.194986	0.176410
5	7	0.183100	0.161456	0.142700
6	6	0.151526	0.130023	0.111811
7	5	0.121032	0.100496	0.083602
8	4	0.091613	0.072995	0.058250
9	3	0.063537	0.047938	0.036208
10	2	0.037457	0.026122	0.018229
11	1	0.014788	0.008992	0.005469
12	0	0	0	0

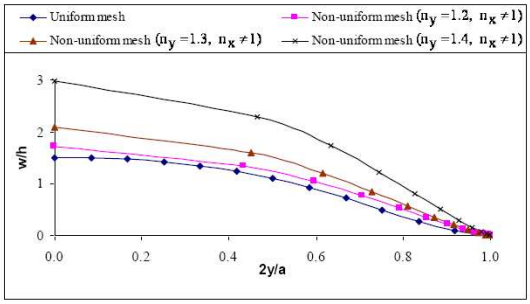

(a)

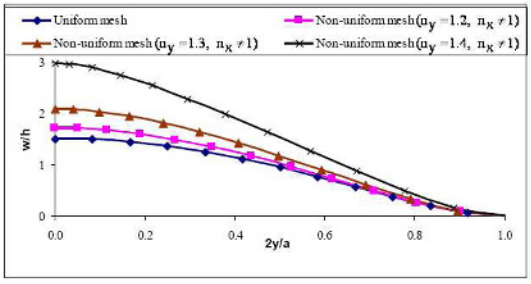

(b)

Fig. 8. Deflection profiles along the y axis of a square orthotropic clamped plate subjected to uniform transverse pressure computed using uniform and a range of non-uniform meshes: (a) principal axis of orthotropy in the x direction; (b) principal axis of orthotropy in the y direction.

have been analyzed using uniform and non-uniform meshes defined by n_y = 1.2, 1.3 *and* 1.4 . Here, $n_x \neq 1$ and it is calculated from Eq. (3) for each mesh line (k = 12). Table 2 shows the n_x values for n_y = 1.2, 1.3 *and* 1.4 . The deflection profiles along the y axis obtained with the uniform and non-uniform meshes are shown in Fig. 8. It is clear that as the exponent n_y increases the non-uniformity of the mesh increases and the calculated deflections are over-estimated compared to the values obtained from the uniform mesh analyses. For example, when $n_y = 1.4$ the mid-span deflection is about twice of that predicted with the uniform mesh.

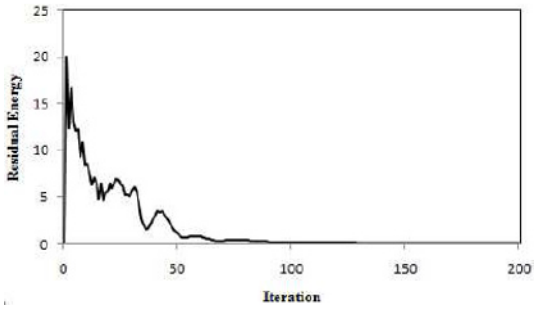

(a)

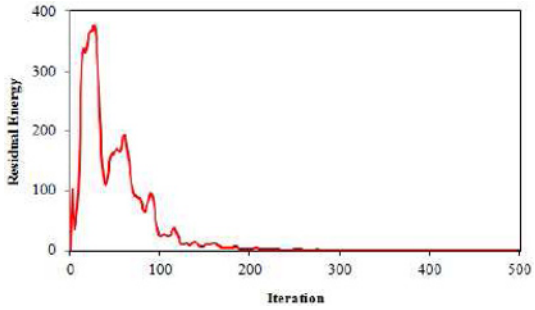

(b)

Fig. 9. A comparison between the convergence rate of two different meshes: (a) Type 1 mesh; (b) mesh with n_y = 1.4.

Generally the mesh used to analyze the orthotropic curved boundaries should have adequate accuracy as well as satisfactory convergence rate. As aforementioned, the Type 1 mesh could provide sufficient accuracy in almost all cases. Furthermore, this type of mesh could also give higher convergence rate. The Figs. 9(a) and 9(b) show the variation of residual energy with iteration number for Type 1 mesh and for the mesh with n_y = 1.4, respectively.

The non-uniform mesh may not just be used to analyze square isotropic and orthotropic plates. It may also be used to analyze isotropic and orthotropic circular and elliptical plates. It is assumed that the axes of orthotropy are parallel to the x and y axes. In order to demonstrate the flexibility and accuracy of the Type 1 mesh the large deflection response of a clamped isotropic circular plate subjected to uniform transverse pressure is analyzed. The center deflection-pressure response is shown in Fig. 10 and compared with the results given in Ref. [18] and also with the results obtained by using a DXDR polar co-ordinate finite-difference analysis of the problem.

In order to demonstrate the ability of the Type 1 mesh for both the small and large deflection responses of clamped orthotropic circular plates, two further results comparisons are presented for a glass-epoxy plate. A small deflection analysis of the load-deflection response for the case of uniform trans-

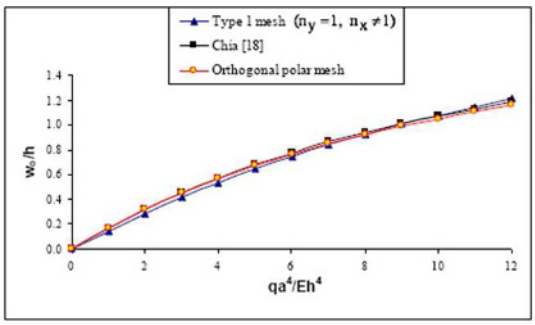

Fig. 10. Load-center-deflection response of a clamped isotropic circular plate subjected to uniform transverse pressure, comparison of Type 1 mesh ($n_y = 1,\ n_x \neq 1$) and other approximate responses.

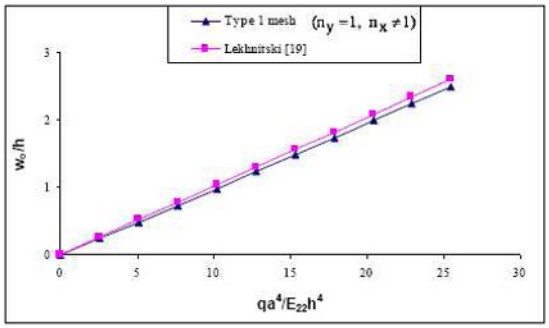

Fig. 11. Small deflection analysis of the load-center deflection response of a clamped orthotropic circular plate subjected to uniform transverse pressure, comparison of Type 1 mesh ($n_y = 1,\ n_x \neq 1$) and exact responses.

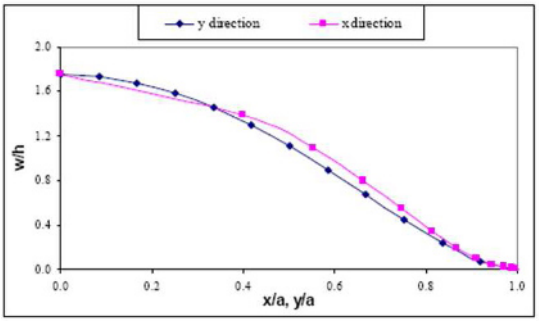

Fig. 12. Deflection profiles along the x and y axes of a clamped orthotropic circular plate subjected to uniform transverse pressure, profiles computed with a Type 1 mesh ($n_y = 1,\ n_x \neq 1$) with the major axis of orthotropy parallel to the y axis.

verse pressure loading is shown in Fig. 11. As expected, the load-deflection response is linear and the Type 1 mesh results are in good agreement with the exact results given in Ref. [19]. Large deflection analysis results for the Type 1 mesh are shown in Fig. 12. The deflection profiles in the x and y directions are presented for the principal axes of orthotropy parallel to the y direction with the non-uniformity of the

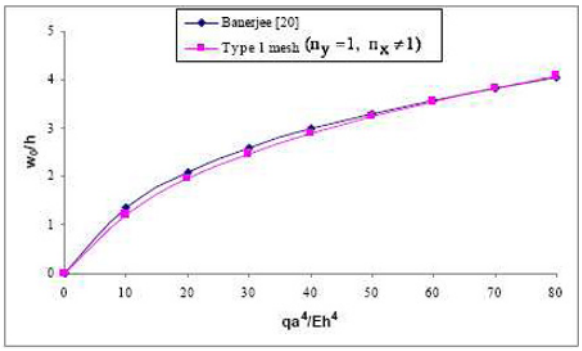

Fig. 13. Large deflection of the load-center deflection response of a movable clamped isotropic circular plate subjected to uniform transverse pressure, comparison of Type 1 mesh ($n_y = 1,\ n_x \neq 1$) and approximate responses.

mesh in the x direction, Type 1 mesh.

The Type one mesh is also capable to investigate the circular and elliptical plates with movable boundary condition in both fixed and simply-supported cases. Fig. 13 shows the large deflection analysis of a movable clamped isotropic circular plate subjected to uniform transverse pressure. As it is seen, there is a good agreement between the results obtained using the Type 1 mesh ($n_y = 1,\ n_x \neq 1$) and the Banerjee results [20]. Moreover, the employed mesh can also be used to analyze the isotropic elliptical plates. The results obtained by the aid of current study and those of Banerjee [21] are compared to each other in Figs. 14(a)-15(a) for movable clamped and simply-supported edges, respectively. Figs. 14(b)-15(b) and 14(c)-15(c) show the profiles along the x and y axes and the stress couple profiles along the x axis for the elliptical plate for the mentioned boundary conditions.

Furthermore, the method can be extended to analyze the large orthotropic circular and elliptical plates with clamped and simply-supported movable edges. Figs. 16 and 17 show the results obtained from current study for glass-epoxy orthotropic plates.

Generally, by the aid of proposed mesh and method explained above it is not only possible to analyze plates with different boundaries but the adequate convergence and accuracy are also achievable. For instance, the Table 3 shows the accuracy of the results which is attainable in this method compared to other published data.

A quick glance at Figs. 4-17 displays the capability of the proposed method and that it could properly treat the circular and elliptical boundaries while Cartesian axes are used. The employed proposed irregular mesh may be applied to any other curved boundaries with more complicated shapes which are especially useful to analyze the orthotropic plates when the reinforced fibers are placed in rectilinear directions. In fact, it quite happens that the reinforced sheets are made initially in large scale and then the plates are cut out with an arbitrary shape and boundary form.

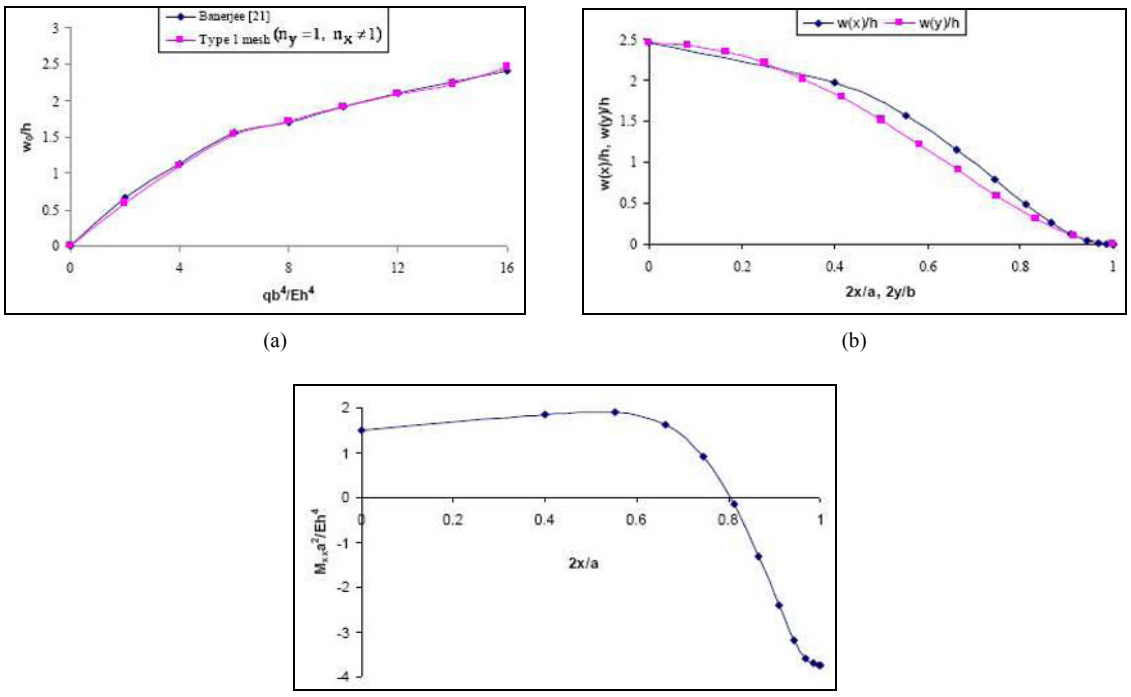

(a) (b)

(c)

Fig. 14. Large deflection analysis of a movable clamped isotropic elliptical plate subjected to uniform transverse pressure (a/b = 2): (a) load-deflection curve and comparison of Type 1 mesh ($n_y = 1,\ n_x \neq 1$) and approximate responses; (b) profiles along the x and y axes; (c) stress couple profiles along the x axis.

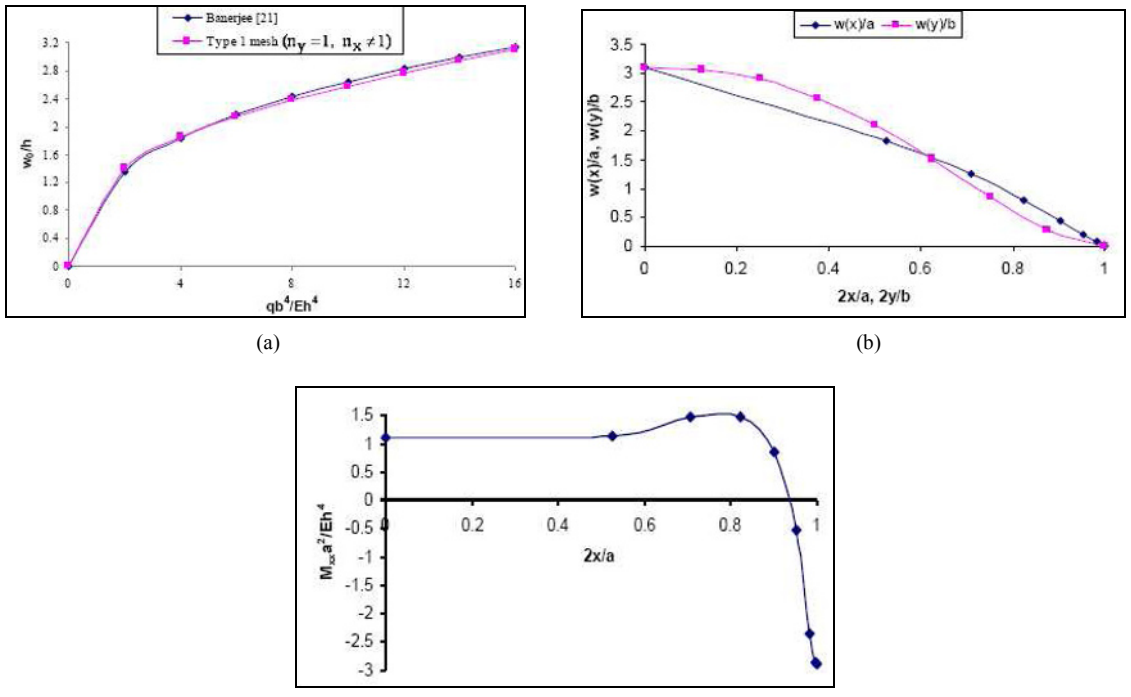

(a) (b)

(c)

Fig. 15. Large deflection analysis of a movable simply-supported isotropic elliptical plate subjected to uniform transverse pressure (a/b = 2): (a) load-deflection curve and comparison of Type 1 mesh ($n_y = 1,\ n_x \neq 1$) and approximate responses; (b) profiles along the x and y axes, (c) stress couple profiles along the x axis.

Table 3. A general comparison between the current results with those of others published data.

Large deflection analysis	Current result	Reference result	Average difference (%)
Square orthotropic clamped plates (Glass-epoxy)	Fig. (5)	Chia [18]	2.74
Clamped isotropic circular plate	Fig. (10)	Chia [18]	2.26
Movable clamped isotropic circular plate	Fig. (13)	Banerjee [20]	2.5
Movable clamped isotropic elliptical plate	Fig. (14)	Banerjee [21]	1.96
Movable simply-supported isotropic elliptical plate	Fig. (15)	Banerjee [21]	0.68

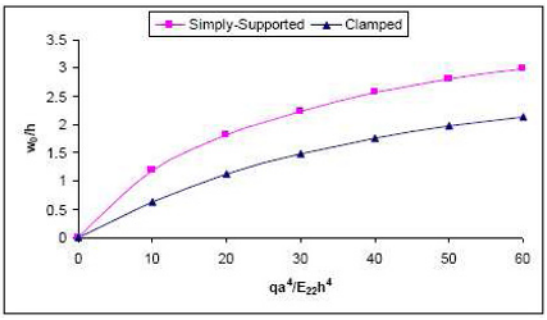

Fig. 16. Large deflection analysis of the load-center deflection response of a movable simply-supported and clamped glass-epoxy orthotropic circular plate subjected to uniform transverse pressure using Type 1 mesh ($n_y = 1$, $n_x \neq 1$).

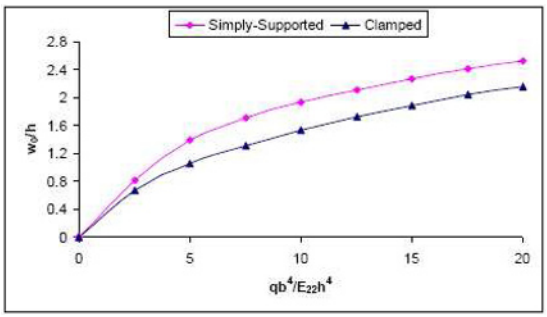

Fig. 17. Large deflection analysis of the load-center deflection response of a movable simply-supported and clamped glass-epoxy orthotropic elliptical plate subjected to uniform transverse pressure using comparison of Type 1 mesh ($n_y = 1$, $n_x \neq 1$).

6. Concluding remarks

Clamped and simply-supported square, circular and elliptical plates with Cartesian orthotropy subjected to uniform transverse pressure have been analyzed using the DXDR technique in conjunction with both uniform and non-uniform Cartesian finite-difference meshes. Both fixed and movable boundary conditions have been investigated. It has been shown that the use of non-uniform finite-difference meshes permits square, circular and elliptical plate geometries to be analyzed using the same Cartesian mesh. Moreover, both the small and large deflection responses of the plates may be predicted with good accuracy provided the non-uniformity of the mesh is not excessive. It appears that, for orthotropic plates, the Type 1 mesh (non-uniform in one direction only) gives best results when the non-uniformity is transverse to the major axis of orthotropy.

Acknowledgment

The research reported in this paper was carried out during part of the first author's sabbatical leave spent in the Engineering Department at Lancaster University. The first author wishes to record his appreciation to the Iranian Ministry of Higher Education and Ferdowsi University for providing financial support during his sabbatical leave. Authors wish to record their appreciation to the Engineering Department for supporting this research collaboration.

References

[1] C. Y. Chia, Large deflection of rectangular orthotropic plates, ASCE Proceedings, *Journal of the Engineering Mechanics Division*, 98 (5) (1972) 1285-1298.

[2] C. Y. Chia and M. K. Prabhakara, Nonlinear analysis of orthotropic plates, proceedings of the institution of mechanical engineers, *Journal of Mechanical Engineering Science*, 17 (3) (1975) 133-138.

[3] M. Dalaei and A. D. Kerr, Analysis of clamped rectangular orthotropic plates subjected to a uniform lateral load, *International Journal of Mechanical Sciences*, 37 (5) (1995) 527-535.

[4] F. C. Mbakogu and M. N. Pavlovic, Bending of clamped orthotropic rectangular plates: a variational symbolic solution, *Computers and Structures*, 77 (2) (2000) 117-128.

[5] P. Tabakov, V. Verijenko and B. Verijenko, Refined theory for the analysis of laminated orthotropic structures, *Composite Structures*, 62 (3-4) (2003) 435-441.

[6] S. Mistou, M. Karama and M. Sabarots, Experimental and numerical simulations of the static behavior of orthotropic plates, *Measurement*, 30 (3) (2001) 197-210.

[7] K. Bhaskar and B. Kaushik, Analysis of clamped unsymmetric cross-ply rectangular plates by superposition of simple exact double fourier series solutions, *Composite Structures*, 68 (3) (2005) 303-307.

[8] M. Salehi and A. R. Sobhani, Elastic linear and non-linear analysis of fibers-reinforced symmetrically laminated sector mindlin plate, *Composite Structures*, 65 (1) (2004) 65-79.

[9] M. Kadkhodayan, L. C. Zhang and R. Sowerby, Analysis of wrinkling and buckling of elastic plates by DXDR method,

Computers and Structures, 65 (4) (1997) 561-574.

[10] M. Kadkhodayan, Using interlacing and irregular meshes in plate analysis, *Iranian Journal of Science and Technology*, 26 (B3) (2002) 419-430.

[11] J. M. Whitney, Structural analysis of laminated anisotropic plates, Technomic Publishing Company, New York (1987).

[12] L. C. Zhang, M. Kadkhodayan and Y. W. Mai, Development of the maDR method, *Computers and Structures*, 52 (1) (1994) 1-8.

[13] P. Underwood, *Dynamic Relaxation*, in T. Belytshko and T.J.R. Hughes, eds., Computational Method for Transient Analysis, Chapter 5, Elsevier, Amsterdam (1983) 245-256.

[14] W. T. Thomson, Vibration theory and applications, Prentice-Hall, 5th Edition, New York (1997).

[15] S. Qiang, An adaptive dynamic relaxation method for nonlinear problems, *Computers and Structures*, 30 (4) (1988) 855-859.

[16] L. C. Zhang and T. X. Yu, Modified adaptive dynamic relaxation method and its application to elastic-plastic bending and wrinkling of circular plates, *Computers and Structures*, 33 (2) (1989) 609-614.

[17] S. E. Han and K. S. Lee, A study of the stabilizing process of unstable structures by dynamic relaxation method, *Computers and Structures*, 81 (17) (2003) 1677-1688.

[18] C. Y. Chia, *Nonlinear Analysis of Plates*, McGraw-Hill, New York (1980).

[19] S. G. Lekhnitskii, *Anisotropic Plates*, Gordon and Breach Science, New York (1968).

[20] B. Banerjee, Large deflections of circular plates of variable thickness, *International Journal of Solids and Structures*, 19 (2) (1983) 179-182.

[21] G. C. Sinharay and B. Banerjee, A modified approach to large deflection analysis of thin elastic plates, *International Journal of Mechanical Sciences*, 28 (3) (1986) 173-177.

Mehran Kadkhodayan received his B.Sc. and M.Sc. degrees from Tehran University, Iran in 1987 and Ph.D degree from the University of Sydney, Australia in sheet metal forming area in 1996. Currently as a full professor he is working in Ferdowsi University of Mashhad, Iran. He has published about 36 journal papers and more than 50 conference papers.